Reprinted from

WEAR

Wear 208 (1997) 25–35

A comparison of the reciprocating and continuous two-body abrasive wear behavior of solution-treated and age-hardened 2014 Al alloy

D. Odabaş *, Ş. Su

Engineering Faculty, Department of Mechanical Engineering, Erciyes University, Kayseri, Turkey

Received 14 February 1996; accepted 4 October 1996

ELSEVIER

ELSEVIER

Wear 208 (1997) 25–35

WEAR

A comparison of the reciprocating and continuous two-body abrasive wear behavior of solution-treated and age-hardened 2014 Al alloy

D. Odabaş *, Ş. Su

Engineering Faculty, Department of Mechanical Engineering, Erciyes University, Kayseri, Turkey

Received 14 February 1996; accepted 4 October 1996

Abstract

In this study, reciprocating and continuous abrasive wear tests have been performed on solution-treated 2014 Al alloys under similar conditions of load, speed, nominal area of contact and sliding distance in order to compare the two-body abrasive wear behavior for two sliding modes. It has been established that the pattern of wear is similar for the continuous and reciprocating wear. On the other hand, the values of the average roughness of the worn surfaces for the reciprocating wear were higher than those for the continuous wear. This is because the values of the wear loss and the abrasive wear coefficient for continuous wear were higher than those for the reciprocating wear. The differences in wear behavior of the test material for the continuous and reciprocating abrasive wear can be explained in terms of the sliding-distance differences between the continuous and reciprocating motions at the same test conditions and the differing amount of abrasion in the two processes by the loose wear debris. © 1997 Elsevier Science S.A.

Keywords: Abrasive wear; Wear coefficient and reciprocating wear

1. Introduction

A great deal of research on the two-body abrasive wear behavior of aluminum alloys has been carried out experimentally. With hard particles dispersed in a relatively ductile matrix, aluminum-alloy matrix composites possess an ideal structure for wear-resistant materials; recent studies have revealed this concept [1–7]. Thus, it was understood that in addition to the volume fraction and spatial distribution of second-phase particles, wear resistance is largely affected by the strength of the particle–matrix interfaces as well as the mechanical properties of matrix materials [1,2]. Consequently, under the service conditions, particles lose their ability to support the applied load. Second-phase reinforcement may cause no improvement or even a deterioration in the wear properties [3,4]. Wang et al. [5] reported that both SiC particulate- and whisker-reinforced composites exhibited greater wear resistance than the unreinforced aluminum alloy. The whisker reinforcement was more effective than the particulate reinforcement in improving the wear resistance of the matrix alloy.

In addition, Song et al. [6] studied changes in the abrasive wear resistance of aluminum-based composites heat treated for different ageing conditions. They found that the hardness and abrasive wear resistance increase with increasing the ageing temperature to 200 °C, but at 250 °C decrease due to the coarsening of the intermetallic precipitates. The composites with 20 μm SiC particles were slightly more wear resistant than those with 3 μm SiC. In another study, it was shown that most composites exhibit better abrasive wear resistance than the unreinforced matrix alloys, and the impact-abrasive resistance increases with decreasing particle size and increasing volume fraction [7].

In all the investigations discussed, abrasive wear behavior of aluminum alloys have been carried out using pin-on disc or pin-on drum test machines under continuous sliding motion but have neglected the case of reciprocating sliding motion, and any comparison of these has not been performed with the continuous wear motion. However, the rate of reciprocating wear is extremely important since a significant proportion of industrial process machinery operates in this fashion.

This work investigates the abrasive wear behavior of solution-treated and age-hardened 2014 Al alloy under very similar conditions during the reciprocating and continuous

* Corresponding author.

0043-1648/97/$17.00 © 1997 Elsevier Science S.A. All rights reserved
PII S0043-1648(96)07378-4

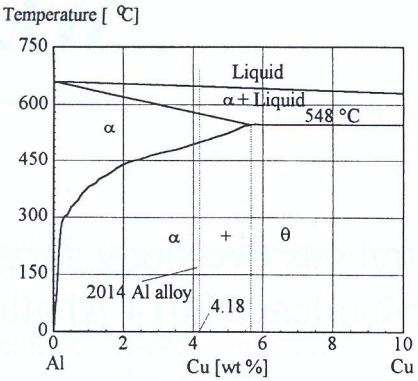


Fig. 1. Al–Cu phase diagram (aluminum-rich portion of the copper–aluminum alloy system).

sliding motion. The abrasive wear tests have been carried out in the two sliding modes using similar speeds, loads, sliding distance, nominal area of contact and abrasive paper.

2. Experimental details

2.1. Material and its preparation

The best-known characteristic of aluminum is its light weight (the density being about one-third that of steel or copper alloys). Some aluminum alloys have a better strength-to-weight ratio than that of high strength steels. In addition, aluminum is suitable for casting and all machining and forming operations; it also has high corrosion resistance, and high electrical and thermal conductivity. The excellent mechanical and tribological properties of aluminum alloys have led to extensive use of these alloys in engineering applications such as plain bearings, internal combustion engine pistons and cylinder liners, aircraft constructions, heavy-duty forgings, and truck frames etc.

The aluminum-rich end of the aluminum–copper equilibrium phase diagram is shown in Fig. 1. The maximum solubility of copper in aluminum is 5.65% at 548 °C and the solubility decreases to 0.45% at 300 °C. Therefore, alloys containing between 2.5 and 5% copper will respond to heat treatment by age hardening. The θ phase is an intermediate-alloy phase whose composition corresponds closely to the compound $CuAl_2$. Solution heat treatment is carried out by heating the alloy into the α single-phase region followed by rapid cooling. Subsequent aging, either natural or artificial, will alloy precipitation of the θ phase thus increasing the hardness and strength of alloy. These alloys may contain smaller amounts of Si, Fe, Mg, Mn, Cr and Zn.

In this study, 2014 Al alloy with higher Cu content was chosen as a test material (Fig. 1). For this test material, chemical analysis (wt.%) was: Cu 4.18; Mn 0.67; Mg 0.72; Si 0.81; Fe 0.26; Zn 0.02 and Ti 0.019 [8]. In general this alloy is used for heavy-duty forgings, aircraft fittings and truck frames. 2014 Al alloy was fabricated by casting in a metal mold at Seydişehir Aluminum Co. in Konya, Turkey. After casting, the homogenization heat treatment was applied to the alloy at 500 °C for 2 h and the hot-pressed billets with a 45 mm diameter were extruded at 450 °C into rods with a 16 mm diameter with an extruded ratio of 3:1. After the rods were left for cooling at the room temperature, they were straightened by a 3% plastic deformation. The specimens were prepared from the rods for the hardness and abrasive wear tests. The specimens to be used for the wear tests were cylinders with a 16 mm diameter and a length of 20 mm while those for the hardness tests were blocks $2.5 \times 8 \times 5$ mm in size. In order to measure the bulk temperature of the pin, a hole 3 mm in diameter was drilled a distance of up to 1 mm from the wear surface of the pin at the center.

Table 1
Solution heat treatments of 2014 Al alloy and final hardness values

Solution heat treatment		After age hardening Final hardness (HB 30)
Temperature (°C)	Time (h)	
400	1	85
450	1	115
475	1	134
490	1	145
505	1	150
520	1	161

Before the wear tests, the specimens were solution treated in a muffle furnace and then quenched in cold water (at 15 °C). Later, the ageing treatment was carried out at 185 °C for 8 h in the furnace. T6 heat-treatment conditions (solution heat treated, artificially aged) and the hardness values are given in Table 1.

2.2. Test methods

Abrasive wear tests in continuous motion were carried out using a grinding–polishing machine with the pin-on disc configuration under dry sliding conditions [Fig. 2(a)]. The disc with 200 mm diameter was driven by an electric motor. The speed of the electric motor is changed by means of an A.C. speed-control converter. The waterproof SiC papers on the rotating disc were used as abrasive materials. The pin specimen (stationary) was mounted in a holder so that it could be removed for measurement and was rubbed against the surface of an SiC paper fixed to the flat surface of a revolving disc. Friction occurred continuously along a single track over which the abrasive ability gradually deteriorated. The radius of a single track was 35 mm. Thus, the average periphery of this track was equal to $2\pi r = 2\pi 35 = 220$ mm. Wear was determined over a friction path of 11 m during the wear test.

Reciprocating abrasive wear tests were carried out using a machine working on a sliding-friction principle [9]. The specimen configuration is illustrated in Fig. 2(b). The waterproof SiC papers were mounted on the lever that was moved in a reciprocating motion in a guide by a crank shaft. The crank shaft was driven by an electric motor whose speed was

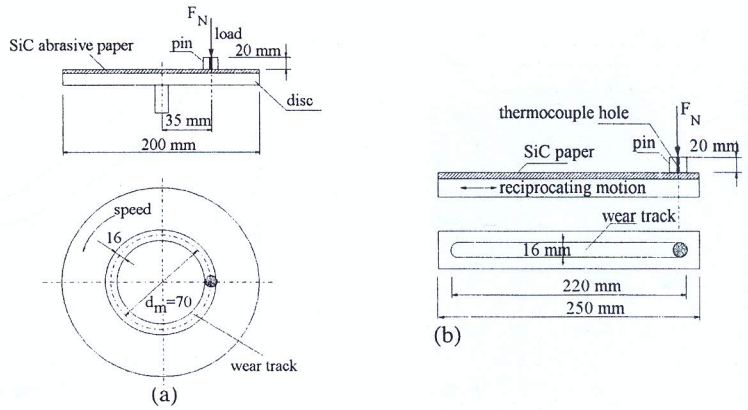


Fig. 2. Schematic test rig: (a) specimen configuration for continuous wear test, (b) specimen configuration for reciprocating wear test.

controlled by using an A.C speed-control converter. The stroke of a reciprocating motion was equal 440 mm (i.e. twice the length of the wear track and which equals $2\times220=440$ mm). The sliding distance was 11 m as the continuous wear. The upper (stationary) pin specimen was mounted in the holder used in the continuous wear tests.

Before the wear tests, the contact surfaces of the pins were polished with 500 grit size SiC paper and the initial average roughness was approximately $R_a=0.06$ μm. Prior to testing, all the specimens were cleaned by rinsing in ethanol and dried in hot air. During the tests, the pin specimens were loaded with dead weights and tests were conducted dry, at room temperature and room humidity. The wear loss was measured by means of an analytical balance with an accuracy of 0.1 mg. The wear surfaces, wear debris and subsurface deformation were also studied in optical and scanning electron microscopes.

The abrasive wear coefficient (k_a) was calculated using the general equation for adhesive and abrasive wear [10], which takes the form $k_a=(VH)/(F_NL)=(GH)/(\gamma F_NL)$. Where G is weight loss, H is the hardness of the softer material, F_N is the load, L is the sliding distance and γ is the density of test material (for a 2014 Al alloy, γ is 2800 kg m^{-3}).

3. Results

3.1. The solution-heat treatment and microstructure

As shown in Table 1, solution treatment of the 2014 Al alloy was carried out at temperatures of 400, 450, 475, 490, 505 and 520 °C for 1 h in a muffle furnace. The dependence of hardness on solution-treating temperature is shown in Fig. 3. The hardness was increased by the increasing the temperature because the solubility of copper in aluminum increased markedly with solution-treating temperature. During quenching, this Cu was retained in solution. Thus, the Al-rich phase (α) would contain Cu in a supersaturated solid solution at room temperature. In the ageing, fine particles of $CuAl_2$ formed and precipitated in solution Fig. 4. Thus, the

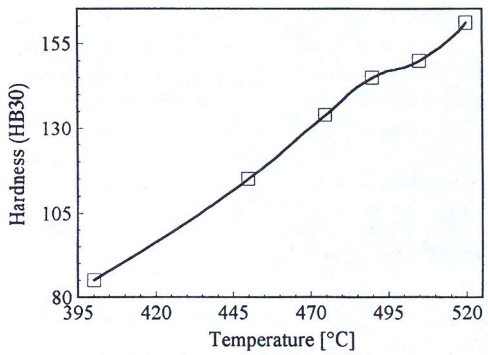


Fig. 3. Dependence of hardness on solution-treating temperature.

hardness of alloy increased by means of artificially age hardening. As shown in Fig. 4, the structure consisted mainly of dark, insoluble particles of a complex compound of Fe, Mn, Si and Al, and a few particles of $CuAl_2$ (white) in a matrix of α solid solution. At 520 °C, there would be partial melting (burning) as shown in Fig. 4(c).

3.2. The effect of the solution-treating temperature on the abrasive wear behavior

The variation in wear loss with solution-treating temperature for both the continuous and reciprocating abrasive wear is plotted in Fig. 5 for a speed of 0.18 m s^{-1}, a sliding distance of 11 m, a load of 5 N using 320 grit abrasive papers. A sliding speed of 0.18 m s^{-1} for the reciprocating test is an average speed given as $V_m=n_L\times[\text{a stroke long}]/(60\times1000]=(25\times440\text{ mm})/(60\times1000)$ (m s^{-1}); this average speed for continuous tests was calculated as $V_m=(\pi d_m n)/(60\times1000)=\pi70\text{ mm}\times50\text{ rpm}/(60\times1000)$ (m s^{-1}); the details are given in Section 4.1. It can be seen from Fig. 5 that the wear loss decreased with increasing the solution-treating temperature. The reason for this may be related to an increasing of the hardness by the solution heat treatment. The hardening capability of 2014 Al alloy was a function of solution-treating temperature as shown in Fig. 3. As a result, it can be accepted that the solution temperature determines the hardness and abrasive wear resistance of 2014 Al alloy. It is clear that the general pattern of wear for the continuous wear

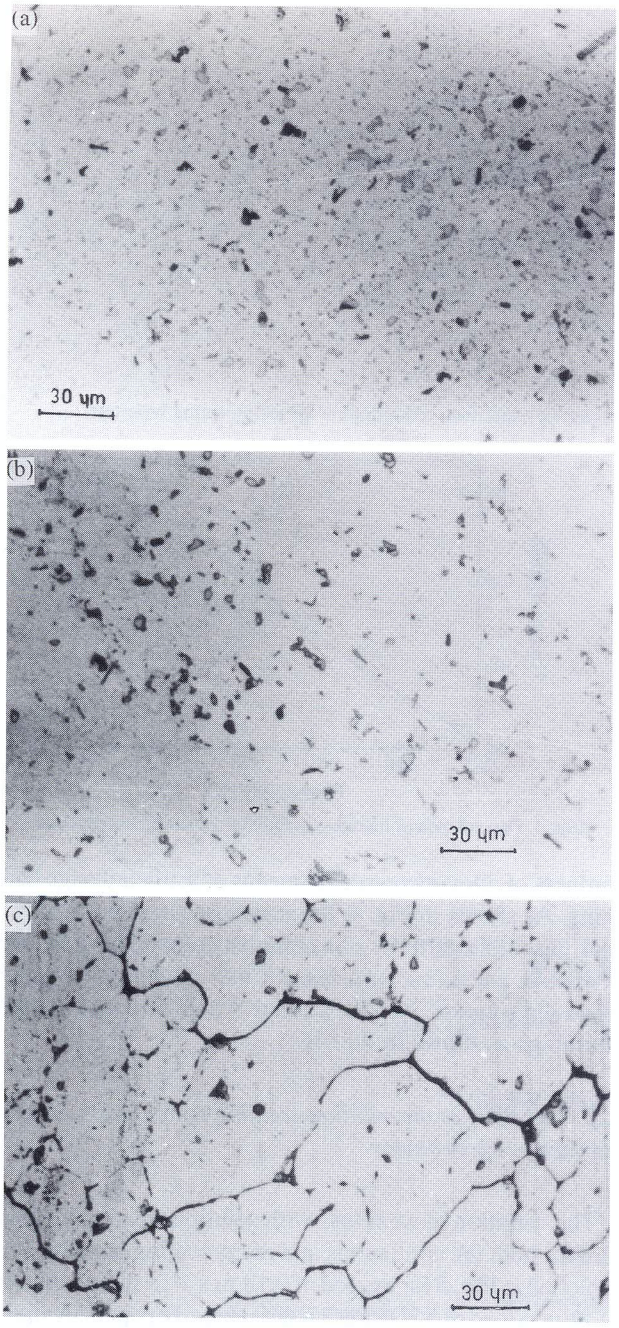


Fig. 4. Microstructure of solution-treated 2014 Al alloy after ageing treatment (solution-treatment duration = 1 h, etched in Keller's reagent): (a) solution-treating temperature of 400 °C (mag. ×500); (b) solution-treating temperature of 470 °C (mag. ×500); (c) solution-treating temperature of 520 °C (mag. ×500).

is similar to that for the reciprocating wear as shown in Fig. 5. However, the values of the wear loss for the continuous motion were higher than those of the reciprocating wear.

Fig. 6 shows the relationship between the abrasive wear coefficient and the solution temperature. It can be seen from this figure that, in general, the wear coefficient increased with an increase in the temperature because of increasing the hardness of the test material. On the other hand, the values of

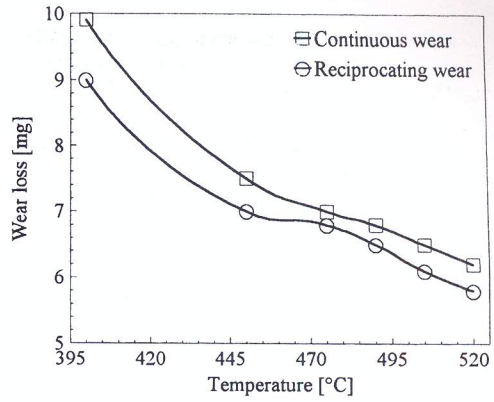


Fig. 5. The variation in wear loss with solution-treating temperature.

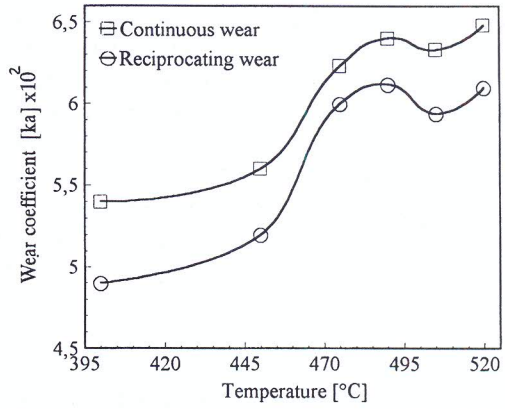


Fig. 6. The variation in abrasive wear coefficient with solution-treating temperature.

wear coefficient for the continuous motion was higher than those for the reciprocating motion.

At the end of each test, the average roughness of the worn surface was measured in a perpendicular direction to the wear tracks by a stylus surface profilometer. Two wear tests for each sliding condition were performed on the same sample. Each value of R_a was averaged from a total of 12 measurements of the two tests. The results are given in Table 2. Fig. 7 shows the effect of the solution-treating temperature on the roughness average for both motion modes. The surface roughness decreased with increasing temperature; the oscillations in roughness are not important. It is enough to understand the general trend of the variation in roughness with temperature. The general trend for the two sliding motions was similar.

3.3. The effects of the abrasive grit size on the wear behavior of 2014 Al alloy

In order to determine the effects of abrasive grit size on the wear behavior of the 2014 Al alloy, five grades of abrasive papers were used as the counterparts, e.g. 18 μm (600 grit), 23 μm (500 grit), 30 μm (400 grit), 35 μm (320 grit), 70 μm (220 grit) and 100 μm (150 grit) SiC paper. Abrasive wear tests were carried out at a load of 5 N, a sliding distance of 11 m, a duration of 60 s and an average speed of

Table 2
The influence of solution-treating temperature on the abrasive wear behavior

Temperature (°C)	Continuous wear			Reciprocating wear		
	Weight loss G (mg)	Average roughness R_a (μm)	Wear coefficient $k_a \times 10^{-2}$ (nondimen.)	Weight loss G (mg)	Average roughness R_a (μm)	Wear coefficient $k_a \times 10^{-2}$ (nondimen.)
400	9.9	1	5.4	9	1.22	4.9
450	7.5	1.13	5.6	7	1.20	5.2
475	7	0.92	6.23	6.8	1.20	6
490	6.8	1.10	6.4	6.5	1	6.12
505	6.5	1	6.33	6.1	1.14	5.94
520	6.2	0.91	6.48	5.8	1	6.1

Table 3
The influence of abrasive grain dimension on the abrasive wear behavior

Abrasive particle diameter (μm)	Continuous wear			Reciprocating wear		
	Weight loss G (mg)	Average roughness R_a (μm)	Wear coefficient $k_a \times 10^{-2}$ (nondimen.)	Weight loss G (mg)	Average roughness R_a (μm)	Wear coefficient $k_a \times 10^{-2}$ (nondimen.)
18	6.5	0.50	6.1	6.2	0.52	5.8
23	7.3	0.60	6.9	6.9	0.65	6.5
30	8.1	0.75	7.6	7.8	0.82	7.3
35	9.6	0.93	9	9	1.04	8.5
70	10	1.34	9.4	9.1	1.63	8.6
100	10.6	1.89	10	10	2.10	9.4

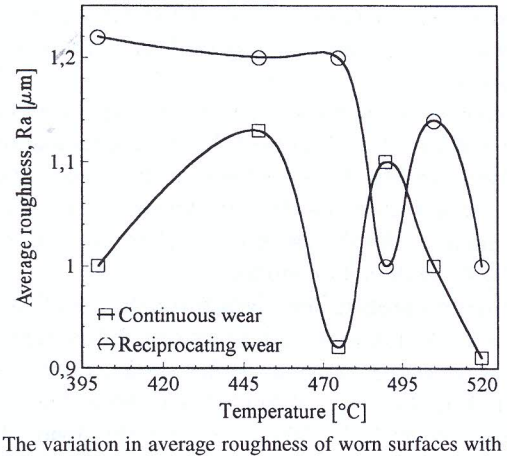


Fig. 7. The variation in average roughness of worn surfaces with solution-treating temperature.

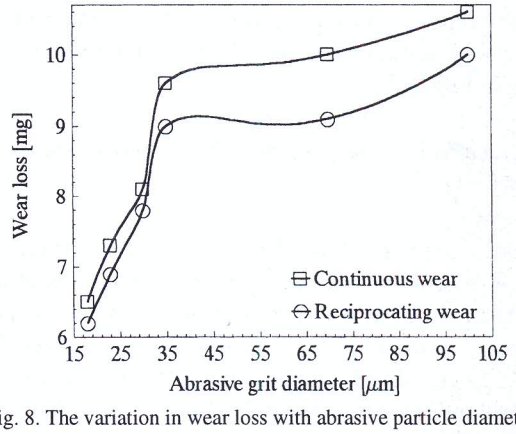


Fig. 8. The variation in wear loss with abrasive particle diameter.

0.18 m s^{-1}. The specimens solution treated at 490 °C for 1 h were used as a test material. After each test, the average roughness of the worn surfaces of the pins was measured perpendicular to the sliding direction by using a stylus surface profilometer. Each value of R_a was averaged from 12 measurements. All the test results are given in Table 3.

As shown in Fig. 8, the wear loss increased with increasing abrasive particle diameter. In particular, the wear loss of the test material increased rapidly in the range 18–35 μm. Beyond a diameter of about 35 to 100 μm, the wear loss increased only moderately with a further increase of grit size. As is well-known, the performance of abrasives is greatly affected by the size of the abrasive grit; the cutting rate of larger abrasive grits is higher than those of the finer grits. With continuous use, the deterioration in cutting rate is much more rapid with finer grit sizes than with coarser. Thus, more inherent cracks in the finer grit sizes results in more grits fracturing during their few cutting traverses and the length of contact of an abrasive particle decreases with decreasing grit size. Thus, in the present sudy, the wear-loss decreased slightly with decreasing grit size, to a critical size of 35 μm, and then decreased steeply. On the other hand, the abrasive wear coefficient of the solution-treated 2014 Al alloy increased with increasing the abrasive particle diameter, as shown in Table 3. If the graph of wear coefficient vs. abrasive

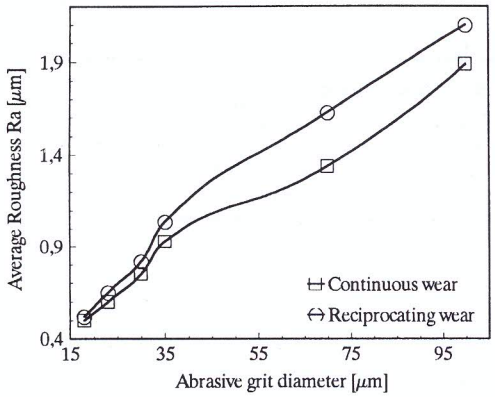


Fig. 9. The variation in average roughness of worn surfaces with abrasive grit diameter.

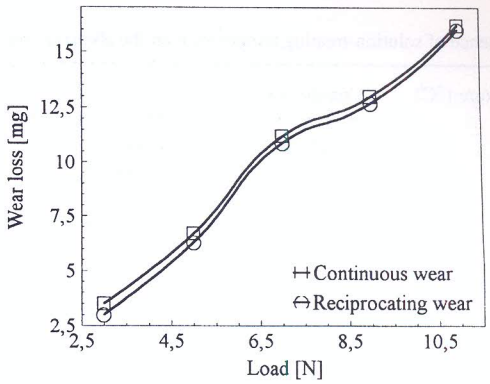


Fig. 10. The dependence of wear loss on load.

particle diameter is drawn, the variation trend of this graph will be very similar to the graph of wear loss vs. abrasive particle diameter. Thus, it was determined that the abrasive wear coefficient of the 2014 Al alloy was strongly dependent on the abrasive grit size.

It is obvious that there is a relationship between the average surface roughness of worn surfaces and the diameter of the abrasive particle, as shown in Fig. 9. The surface roughness increased with increasing the particle diameter (i.e. grit size). In addition, the roughness values at the abrasive particle diameters between 18 and 35 μm were approximately equal for both the continuous and reciprocating wear processes. The difference between the values of roughness increased greatly with an abrasive particle diameter over 35 μm, as shown in Fig. 9.

3.4. The effects of load on the abrasive wear behavior of 2014 Al alloy

In order to understand the variation in wear behavior with load for the continuous and reciprocating motion, wear tests were carried out at a sliding distance of 11 m, a speed of 0.36 m s^{-1}, a duration of 30 s and loads in the range 3–11 N using 220 grit abrasive paper under dry friction conditions. The specimens solution treated at 520 °C for 1 h were tested. The results were given in Table 4.

Fig. 10 shows the dependence of wear loss on the load. It is shown clearly in this figure that the values of wear loss for the continuous wear were higher than for the reciprocating wear. Generally, wear loss increased linearly with increasing loads. However, the wear loss was directly proportional to the load up to a critical load of 7 N. After this load, the slope of the curves decreased for both the continuous and reciprocating wear because the excessive deformation of the worn surface and the instability of the abrasive grains began to increase [11]. When the load on an abrasive grain reaches a critical value, the groove width is about 0.17 of the abrasive grain diameter, and the abrasive grains begin to fail. Thus, groove widths are fairly constant with load but the number of contact points increases linearly with load. If grit wear can be eliminated, the wear loss may be directly proportional to the applied load.

For comparison purposes, the abrasive wear coefficient is plotted against the load for both the continuous and reciprocating wear in Fig. 11. As shown in this figure, the wear coefficient increased linearly with increasing load, reached a maximum at a critical load of 7 N and then decreased exponentially for both motion modes.

In order to analyze the surface roughness of the worn surfaces for both motions, after each test, the average roughness was measured by using a stylus surface profilometer. It is clear from Table 4 and Fig. 12 that the average surface roughness decreased with increasing the load. This is

Table 4
The influence of the load on the abrasive wear behavior

Load (N)	Continuous wear			Reciprocating wear		
	Weight loss G (mg)	Average roughness R_a (μm)	Wear coefficient $k_a \times 10^{-2}$ (nondimen.)	Weight loss G (mg)	Average roughness R_a (μm)	Wear coefficient $k_a \times 10^{-2}$ (nondimen.)
3	3.5	1.62	6.1	3.0	1.78	5.2
5	6.7	1.34	7.0	6.3	1.63	6.6
7	11.2	1.00	8.4	10.9	1.23	8.1
9	13.0	0.98	7.5	12.7	1.00	7.4
11	16.2	0.85	7.7	16.0	0.93	7.6

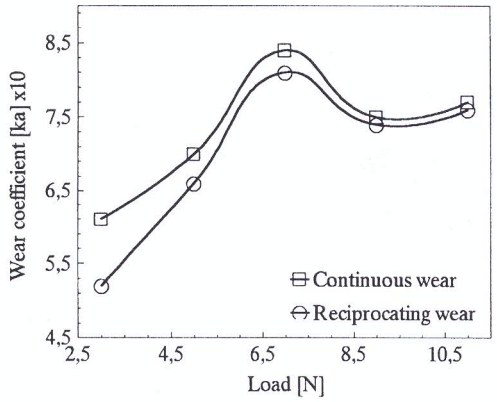


Fig. 11. The dependence of abrasive wear coefficient on load.

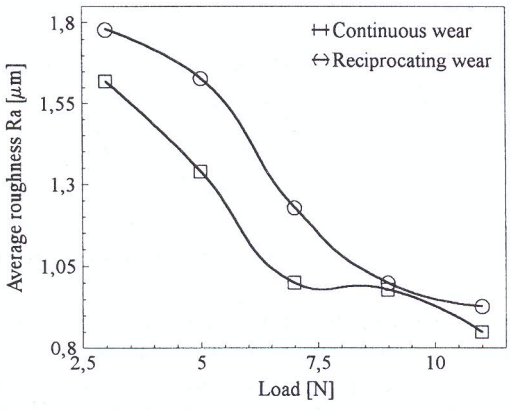


Fig. 12. The dependence of average roughness of worn surfaces on load.

explained by the fact that that the failure rate of the abrasive particles increased and the grit size decreased inversely proportional with load. The values for the reciprocating wear were higher than for the continuous wear.

3.5. *The effect of the sliding speed on the abrasive wear behavior of 2014 Al alloy*

In this section, in order to compare the variation in the wear loss of the 2014 Al alloy with sliding speed for both the continuous and reciprocating motions, all the abrasive wear tests were performed at a speed range 0.09–0.90 m s^{-1}, a load of 5 N and an average sliding distance of 11 m using abrasive papers of 150 grit size. A test material solution

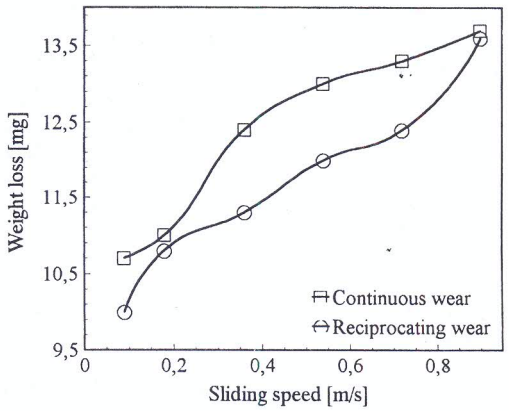


Fig. 13. The variation in wear loss with sliding speed.

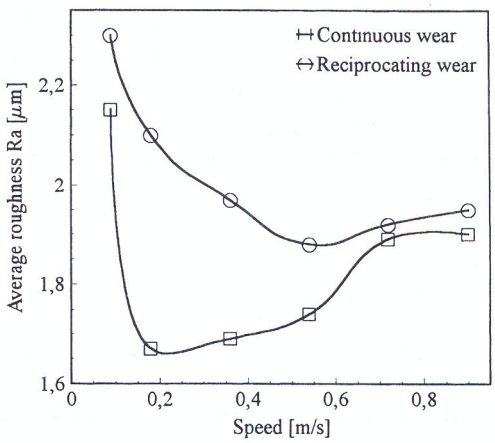


Fig. 14. The variation in average roughness with speed.

treated at 505 °C for 1 h was used during the wear tests. The results are given in Table 5.

Fig. 13 shows that the wear loss increased slightly as the sliding speed increased in the range 0.09–0.90 m s^{-1}. The reason for this is that changes arising from strain rate and friction heating are expected with increasing sliding speeds [11].

It was determined that the abrasive wear coefficient increased by increasing the speed as shown in Table 5. In addition, if the variation graph of wear coefficient with speed is drawn, the general pattern of the wear coefficient would be similar to that for wear loss under both motion modes. How-

Table 5
The influence of the sliding speed on the abrasive behavior

Speed (m s^{-1})	Continuous wear			Reciprocating wear		
	Weight loss G (mg)	Average roughness R_a (μm)	Wear coefficient $k_a \times 10^{-2}$ (nondimen.)	Weight loss G (mg)	Average roughness R_a (μm)	Wear coefficient $k_a \times 10^{-2}$ (nondimen.)
0.09	10.7	2.15	10.3	10.0	2.30	9.5
0.18	11.0	1.67	10.4	10.8	2.10	10.3
0.36	12.4	1.69	12.0	11.3	1.97	10.7
0.54	13.0	1.74	12.3	12.0	1.88	11.5
0.72	13.3	1.89	12.6	12.4	1.92	11.8
0.90	13.7	1.90	13.1	13.6	1.95	13.0

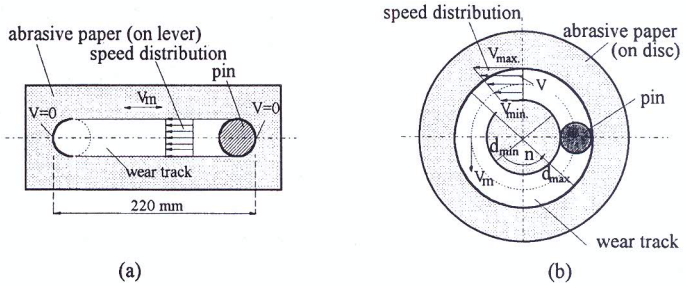


Fig. 15. The distribution of speed on a wear track for both motion modes: (a) the speed distribution for reciprocating motion, (b) the speed distribution for continuous motion.

ever, the values of k_a for the continuous wear were higher than for the reciprocating wear.

On the other hand, it is apparent from Fig. 14 that the average roughness of the worn surface of the pins decreased with increasing speed, reached a minimum at a speed of 0.18 m s^{-1} for continuous motion and at a speed of 0.54 m s^{-1} for reciprocating motion, and then increased at a constant level. It is evident that the roughness values for the continuous wear are smaller than for the reciprocating wear.

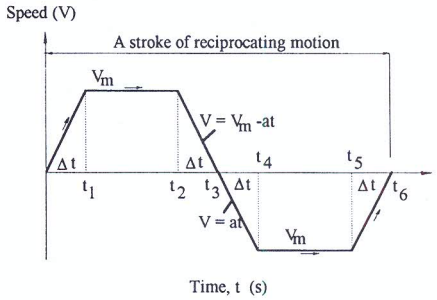


Fig. 16. The variation in speed with duration of a reciprocating stroke.

4. Discussion

The basic differences that exist between the continuous and the reciprocating abrasive wear will first be considered in order to decide those differences that could be responsible for the observed differences in abrasive wear behavior of the solution-treated 2014 Al alloy.

4.1. Speed changes in the continuous and reciprocating motion

As shown in Fig. 15(a), the distribution of speed on a wear track is uniform in the reciprocating motion. Every contact area of pin specimen moves at the same speed and the friction path for each contact point against abrasive grits will be the same during the wear process. However, the worn surface of the pin is sheared in the opposite direction alternately. As shown in Fig. 16, the sliding speed accelerates from zero to an average speed of V_m at the beginning of a reciprocating motion stroke during a time interval of Δt between $t=0$ and $t=t_1$. After a time of t_2, the speed decreases to zero at the end of the stroke during the same time interval (i.e. at $\Delta t=t_3-t_2$). Following this, it accelerates again to a similar speed of V_m in the opposite direction at a time interval of Δt (i.e. at $\Delta t=t_4-t_3$). Thus, the speed of reciprocating motion accelerates to a speed of V_m and decreases to zero twice during one stroke of the reciprocating wear. The slope of the speed curve is constant because the acceleration (a) was assumed to be constant.

The average speed between $t=0$ and $t=t_1$ was given as $V=(1/2)V_m=(1/2)at_1$. The acceleration was defined as $a=V_m/\Delta t$. The average sliding speed for all wear tests was calculated as $V_m=[n_L\times(\text{a stroke long})]/60\times1000$ $=[n_L\times(440\text{ mm})]/60\times1000$ where n_L is the stroke number of the reciprocating motion per minute.

The loss of the sliding distance for a stroke of reciprocating motion can be given as $s=(1/2)V_m(4\Delta t)=2V_m\Delta t$ (Here, it is assumed that $\Delta t=t_1=t_3-t_2=t_4-t_3=t_6-t_5$.) The total sliding distance for all tests was given as 11 m and the total stroke number was equal to $n_t=11\text{ m}/0.44\text{ m}=25$ strokes. During the reciprocating wear, the total real sliding distance can be calculated as $l_r=11-s\times n_t=11-2V_m\times\Delta t\times(25)=11-50V_m\times\Delta t$. The time interval ($\Delta t$) can be calculated as $\Delta t=V_m/a$. The values of acceleration were measured by using an electronical accelerometer. All results are given in Table 6.

The speed distribution on a wear track for continuous motion is not uniform as shown in Fig. 15(b). The speed distribution has a linear line and the average sliding speed was calculated as $V_m=(\pi d_m\times n)/60\times1000$ (m s^{-1}) where n is the number of revolutions per minute of the disc and d_m (70 mm) is the average diameter of the circular motion [Fig. 2(a)]. However, the average speed changes between a minimum speed of V_{min} and a maximum speed of V_{max}. The minimum speed and maximum speed were calculated as $V_{min}=(\pi d_{min}n)/(60\times1000)$ and $V_{max}=(\pi d_{max}n)/60\times1000$, respectively. The values of d_{min} and d_{max} are 62 and 78 mm, respectively, as shown in Fig. 2(a).

On the other hand, in the continuous wear, the center of the worn surface of the pin moves with an average speed of V_m and the total average sliding distance is given as $L=V_m.t=11$ m where t is the duration of the test. One half of the worn surface of the pin moves with a minimum speed of V_{min} and the minimum sliding distance is equal to $L_{min}=V_{min}.t=9.6$ m. Similarly, the other half of the worn surface moves with a maximum speed of V_{max} and the max-

imum distance is given as $L_{max} = V_{max}t = 12.24$ m. The results are given in Table 6.

The factor of the sliding speed distribution for both continuous and reciprocating wear can be regarded as significance on the two-body abrasive wear behavior of the 2014 Al alloy. As shown from the results in Table 6, the sliding distance changes between 9.6 and 12.24 m for continuous wear and between 8.75 and 10.11 m for reciprocating wear. Thus, the distance values of continuous motion were always higher than those of reciprocating motion. Therefore, a higher wear loss would be expected in continuous wear than in reciprocating wear at the same test conditions used in the present study as shown in Figs. 5, 8, 10 and 13.

4.2. Wear debris

A schematic diagram of the wear mechanism in two-body abrasive wear is shown in Fig. 17. Wear particles removed from the pin specimen surface consist of two kinds of particles, i.e. particles transferred to the surface of the abrasive paper disc and cutting-type wear particles removed as metal chips. On the contrary, the abrasive grains removed from the abrasive paper because of chipping, dislodgement and so forth, are given the general name ''dislodged abrasive grains'' [12].

In both the continuous and reciprocating motions, friction between pin and abrasive particles occurs a long a single wear track. During reciprocating wear, some of the wear particles and the dislodged abrasive grains are picked up in front of the pin and removed from the rubbing system. During continuous motion, however, these wear particles are trapped between the sliding surfaces for much longer. After the first few cutting traverses, some of the abrasive grains fracture rapidly and their grit size decreases. During friction, the deterioration in the size of the abrasive grains in the continuous motion is higher than in the reciprocating motion, and the abrasive ability decreases more. Therefore, the grit size of the wear particles and the dislodged abrasive grains for continuous wear is smaller than for reciprocating wear, and the values of average roughness of the worn surface of the pin for continuous wear were lower than for reciprocating wear, as shown in Figs. 7, 9, 12 and 14. The reason for this may be that the wear-groove depth of the worn surface decreases with decreasing the grain dimension. Fig. 18 shows the optical micrographs of the worn surfaces of pin specimen after the abrasive wear tests. The grooves in the worn surface for the reciprocating wear were larger than those for the continuous wear [Fig. 18(b)]. The worn surface for the continuous wear had the narrowest grooves [Fig. 18(a)].

X-ray diffraction studies of the wear debris obtained during tests were made. This analysis showed that the wear debris consisted of SiC, Al, $CuAl_2$, Mn and Si. The wear surfaces, wear debris and subsurface deformation were also studied using a scanning electron microscope for both continuous

Table 6
The results of dynamic analysis for both continuous and reciprocating motion

t (s)	V_m [a] (m s^{-1})	Continuous motion			Reciprocating motion				
		n (rpm)	V_{min} [b] (m s^{-1})	V_{max} [c] (m s^{-1})	n_L (strokes min^{-1})	$t_6 = 60/n_L$ (s)	a (m s^{-2})	Δt (s)	L_r (m)
120	0.09	25	0.08	0.102	12	5	0.09	1	8.75
60	0.18	50	0.16	0.204	25	2.4	0.45	0.4	9.2
30	0.36	100	0.32	0.408	50	1.2	2	0.18	9.38
20	0.54	150	0.48	0.612	75	0.8	5.4	0.10	9.65
15	0.72	200	0.64	0.816	100	0.6	12	0.06	9.92
12	0.90	250	0.8	1	125	0.48	22.5	0.04	10.11

[a] $L_m = 11$ m
[b] $L_{min} = 9.6$ m
[c] $L_{max} = 12.24$ m

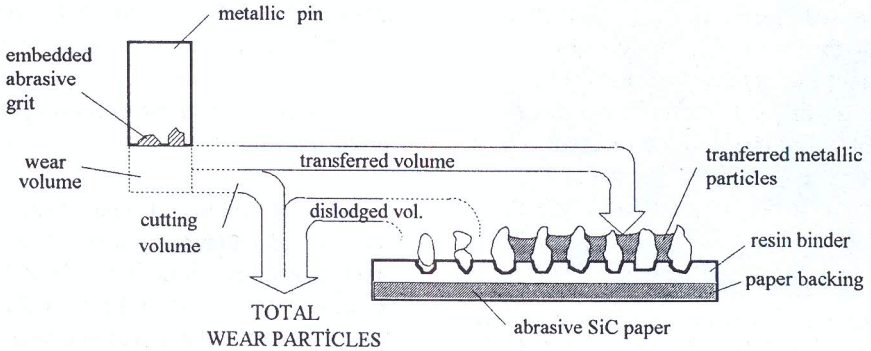


Fig. 17. Schematic diagram of the abrasive wear mechanism [12].

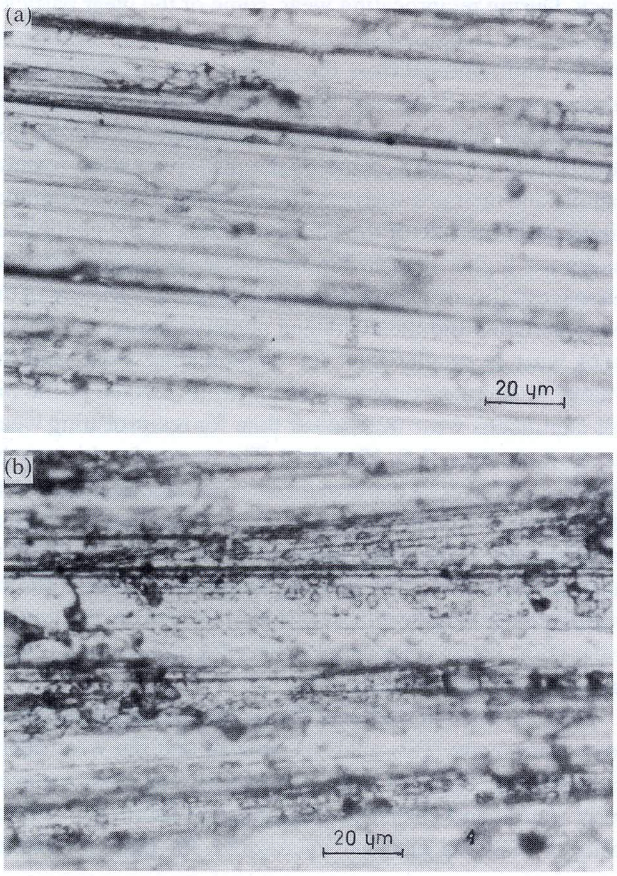


Fig. 18. Optical micrographs of worn surfaces of pins (solution-treating temperature = 505 °C, load = 5 N, sliding speed = 0.18 m s^{-1}, sliding distance = 11 m and abrasive grit size = 150): (a) continuous wear (mag. ×800); (b) reciprocating wear (mag. ×800).

and reciprocating tests. The SiC particles embedded in the worn surface were observed on the surface of the pin in the SEM image, as shown in Fig. 19. However, the volume of SiC grits embedded in the surface layer of the test material can be negligible compared with that of dislodged abrasive grits for both wear modes. Occasionally, SiC particles were also observed in the wear debris. A typical SiC particle in the debris is shown in Fig. 20.

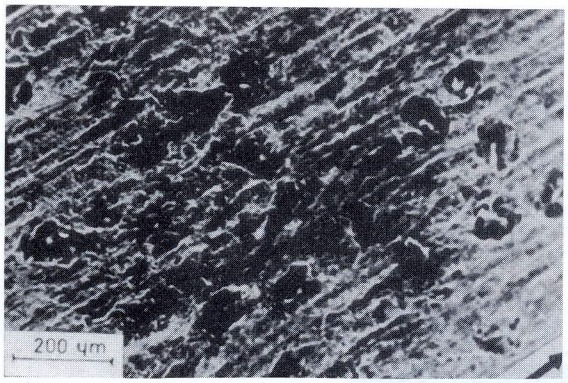


Fig. 19. SE micrograph image of worn surface of 2014 Al alloy for a speed of 0.18 m s^{-1}, 5 N load using 150 grit paper in the continuous test, showing the SiC particles embedded in test material (mag. ×100).

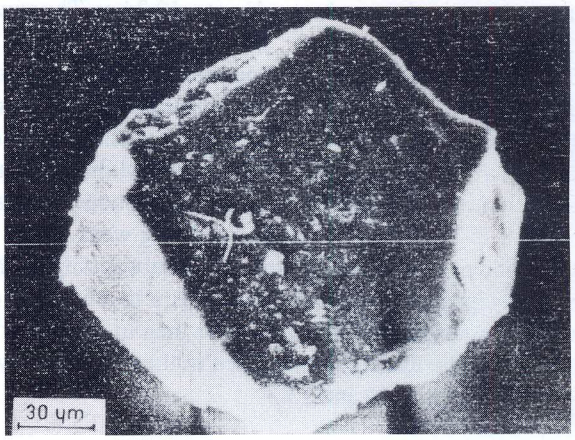


Fig. 20. SE micrograph image of a typical SiC particle in the debris for continuous test (mag. ×500, speed = 0.18 m s^{-1}, load = 5 N, using 150 grit paper).

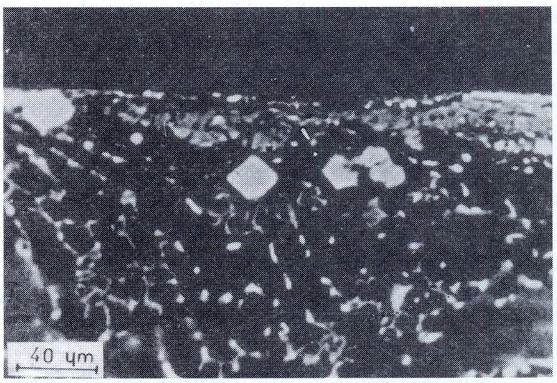


Fig. 21. SE image of the subsurface of worn surface parallel to the sliding directed for a speed of 0.36 m s^{-1} and 11 N load, using 220 grit paper in continuous test (mag. ×400).

Fig. 21 shows the microstructure in cross section through the worn surface of the test material. It can be seen that there are two sections in the microstructure. The topmost part has been found to exhibit an extremely fine microstructure as a result of the large plastic deformation and strain hardening. In addition, the subsurface cracks under the worn surface were nearly continuous in parallel to the sliding direction. On the other hand, the values of wear loss of wear coefficient for continuous motion were higher than for reciprocating motion, as shown in Figs. 5, 6, 8, 10, 11 and 13. The reason for this may be that in the continuous wear all the particles trapped between the contact surfaces acted as third abrasive elements for much longer than in the reciprocating wear.

4.3. The effect of the friction heat from the sliding surfaces on the wear

The heat conducted away from the sliding surfaces is another factor affecting the wear behavior in view of the effect of surface temperature on the wear loss. In order to estimate the effect of the friction heat on the wear behavior, an Fe-constant thermocouple was placed in the center of the pins at a 1 mm distance from the worn surface and the bulk temper-

ature was measured. It was observed that the temperature increased between a minimum temperature of 24 °C and a maximum of 36 °C (The wear tests were conducted at a room temperature of 22 °C.) This factor may be believed to be of little significance in the present study because the test conditions were selected using load–speed combinations at which the surface temperatures are likely to be comparatively low. On the other hand, a specimen holder was designed to give ease of heat conduction from contacting surfaces and the same holder was used in each test apparatus.

5. Conclusions

Although, the general pattern of wear behavior of solution-treated 2014 Al alloys is similar under the reciprocating and continuous wear conditions, the continuous wear differs from the reciprocating wear in the following respects:

1. the wear loss is greater in the continuous wear;
2. the abrasive wear coefficient rate is higher in the continuous wear;
3. the values of average roughness of the worn surfaces are greater in the reciprocating wear.

The above differences between the continuous and reciprocating wear can be explained in terms of the greater sliding distance and the greater amount of abrasion by the loose wear debris trapped between the contact surfaces of the pin and abrasive paper for much longer in the continuous wear.

References

[1] A.G. Wang, I.M. Hutchings, Wear of alumina fiber—aluminum metal matrix composites by two body abrasion, Materials Science Technology 5 (1989) 71–76.
[2] S.J. Lin, K.S. Liu, Effect of aging on abrasion rate in an Al–Zn–Mg–SiC composite, Wear 121 (1988) 1–14.
[3] A.T. Alpas, J.D. Embury, Sliding and abrasive wear resistance of an aluminum 2014–SiC particle reinforced composite, Scripta Metallurgica Materiala 24 (1990) 931–935.
[4] K.J. Bhamsali, R. Mehrabian, Abrasive wear of aluminum–matrix composite, Journal of Metals 34 (1982) 30–34.
[5] A. Wang, H.J. Rack, Abrasive wear of silicon carbide particulate- and whisker-reinforced 7091 aluminum matrix composite, Wear 146 (1991) 337–348.
[6] W.Q. Song, P. Krauklis, A.P. Mouritz, S. Bandyopadhyay, The effect of thermal ageing on the abrasive wear behavior of age-hardened 2014 Al/SiC and 6061 Al/SiC composites, Wear 185 (1995) 125–130.
[7] Y.N. Liang, Z.Y. Ma, S.Z. Li, S. Li, J. Bi, Impact-abrasive behavior of SiC_p/2024 Al composites in single pendulum scratch testing, Wear 178 (1994) 9–15.
[8] Ş. Su, The effects of the solution treating temperature and duration on the mechanical properties of 2014 Al alloy after age hardening, M.Sc. thesis, Selçuk University, Konya, Turkey, (1988).
[9] M.B. Karamiş, D. Odabaş, A simple approach to calculation of the sliding wear coefficient for medium carbon steels, Wear 151 (1991) 23–34.
[10] H.J. Verbeek, Tribological systems and wear factors, Wear 56 (1979) 81–92.
[11] M.A. Moore, A Review of two-body abrasive wear, Wear 27 (1974) 1–17.
[12] T. Hisakado, H. Suda, T. Tsuki, Effects of dislodgement and size of abrasive grains on abrasive wear, Wear 155 (1992) 297–307.